Int. J. Electrochem. Sci., 16 **(2021)** Article Number: 211110, doi: 10.20964/2021.11.25

International Journal of
ELECTROCHEMICAL
SCIENCE
www.electrochemsci.org

Corrosion Behavior of X70 Pipeline Steel in 3.5% Nacl Solution under the Synergistic Action of Cathodic Protection and Sulfate-reducing Bacteria

Lin Teng, Chuan He, Xin Pan, Chang Liu, Xu Chen[*]

College of Petroleum Engineering, Liaoning Petrochemical University, Fushun 113001, China
[*]E-mail: cx0402@sina.com

Received: 27 July 2021 / *Accepted:* 5 September 2021 / *Published:* 10 October 2021

The corrosion behavior of X70 pipeline steel in 3.5% NaCl solution under the synergistic action of cathodic protection (CP) and sulfate-reducing bacteria (SRB) was studied. The growth curves of SRB under various polarization potentials were measured. The results showed that SRB reproduction was suppressed and the bacteria rapidly entered decline phase at an anodic polarization potential. Under the stimulation of cathodic potential of -0.85 V_{SCE}, the reproduction of SRB was promoted. The death of the bacteria was accelerated when CP potential reached -1.0 V_{SCE}. The growth cycle of SRB had significant influence on the CP efficiency. During SRB growth phase, the excess electrons of CP were directly utilized by SRB as electron donors to metabolize. CP current repelled the electronegative SRB, and CP and SRB synergistically mitigate the steel corrosion. When SRB enters the death stage, the metabolite of SRB acted synergistically with CP to promote hydrogen evolution, and CP promoted SRB corrosion.

Keywords: X70 pipeline steel; sulfate-reducing bacteria; cathodic protection; microbial corrosion

1. INTRODUCTION

As one of the most commonly used means to prevent pipeline corrosion, cathodic protection (CP) has been widely accepted[1-3]. A complete coating can prevent pipe from corrosion, but the mechanical damage of pipeline during installation can cause coating defects[4-6]. As a coating loses its adhesion, a gap is formed between the coating and the pipe surface and then water in soil penetrates into the disbonded coating[7-9]. Therefore, a chemical and electrochemical environment leading to localized corrosion and stress corrosion cracking of pipelines is generated[10-12]. In general, the CP system is designed under a potential of -0.85 V_{CSE}, which is considered as the minimum potential to protect metals[13]. This value was determined in several reference documents: NACE RP0169-02, Recommended Practice DNV-RP-401-05, and international standard ISO 15589-1[14]. However,

under certain conditions, like bacteria, are present, the CP potential of -0.950 V_{CSE} is recommended for pipeline steel[14].

Any bacteria in the natural environment, especially sulfate-reducing bacteria (SRB), can change the metals surface characteristic[15], thus affecting the hydrogen evolution reaction and hydrogen absorption[16-18]. It is important in the CP system. SRB, as ubiquitous and diverse anaerobic bacteria, can utilize sulfate ions as terminal electron receptors to produce H_2S[19-21]. The effects of SRB on metal corrosion can fall into two categories - direct corrosion and indirect corrosion[22]. Indirect corrosion is caused by bacterial metabolites, hydrogen sulfide and sulfides[23,24], or the consumption of organic acids[25,26]. Direct corrosion means that SRB skips H_2 generated by the chemical reaction as the electron donor and chooses to directly use electrons on the metal surface to survive[27]. However, when applied potential is present, the effect of SRB activity on the electrode cannot be ignored.

The interaction between CP and microbial activity has been extensively explored. Edyvean [28] found that CP could suppress the deposition and attachment of aerobic microorganisms on both the stainless steel and carbon steel surfaces. They prevented the growth of biofilms by controlling the potential or current. Little et al. [29] studied the interaction between biofilms formed on steel surface and CP and demonstrated that corrosion induced by microorganisms became more aggressive when the cathode current was discontinuous. However, Nekoksa [30] found that CP promoted the enrichment and growth of bacteria and there were more bacteria on the steel surface which cathodically protected than those under open circuit potential (OCP). Shirtliff et al. [31] applied a cathodic current on a stainless steel electrode and instead of reducing the biofilm, the current was found to even increase the number of bacteria. Guan et al. [22] reported that increased bacterial metabolic activity at -0.85 V_{SCE} might be due to the direct electron transfer from the electrode. However, at -1.05 V_{SCE}, the direct electron transfer cannot be realized due to the use of over-negative cathode protection, which resulted in the conversion of sulfide corrosion to carbonate corrosion. Liu [32] believed that CP had no effect on the growth of planktonic bacteria in the medium. The CP promoted the bacteria adhesion and the biofilm formation on the cathodically protected steel, thus reducing the effect of CP. In the solution containing SRB, the steel was unprotected at -0.85 V_{SCE}, and pitting was observed under the biofilm, although uniform corrosion could be controlled by moving CP potential negatively to -1.0 V_{CSE}.

The relationship between CP and microbial influence corrosion is poorly understood. In addition, external corrosion still occurs on the pipeline surface even after the CP system is applied. In many cases, the corrosion of a cathodically protected metal was associated with the presence of microorganisms[14]. In this study, in order to reveal the influence of polarization potential on SRB activity, anodic polarization was also considered. The study will provide the basis for the selection of an appropriate protection potential for pipeline in marine microbial environment.

2. EXPERIMENTAL

2.1 Materials

X70 pipeline steel used in the work are composed of C 0.045, Mn 1.48, Ni 0.16, Cu 0.21, Nb

0.033, Mo 0.23, Cr 0.031, Si 0.26, P 0.017, S 0.001 (wt%) and Fe. The specimens used in immersion were machined to the dimensions of 10 mm × 40 mm × 1 mm. The back of the electrochemical test specimens was welded with wire and sealed with epoxy resin, leaving a working area of 1 cm^2. All specimen surfaces were polished with 80–2000# water sandpaper, washed with distilled water after degreasing with acetone, and dried by N_2.

2.2 Solutions and microbial cells

The experimental solution was 3.5% (wt%) sodium chloride solution, the analytically pure sodium chloride was dissolved in deionized water. The solution was sterilized in a pressure steam sterilizer (steam temperature was 121 ºC) and then stored as a sterile medium at 4 ºC.

The SRB (*Desulfovibrio desulfuricans, 1.5189*) was purchased from China General Microbiological Culture Collection Center (CGMCC). The culture medium in this study was recommended by CGMCC. The Medium I contained (g/L) 0.5 K_2HPO_4, 0.5 Na_2SO_4, 1 NH_4Cl, 0.1 $CaCl_2$, 2 $MgSO_4 \cdot 7H_2O$, 1 yeast extract, and 3 mL of sodium lactate (55 vol%). Next, the medium was autoclaved at 121 °C for 15 min. The nutrient-rich Medium II consists of 0. 1 $g \cdot L^{-1}$ ascorbic acid, 0.1 $g \cdot L^{-1}$ sodium hydrosulfite, and 0.1 $g \cdot L^{-1}$ $(NH_4)_2Fe(SO_4)_2 \cdot 6H_2O$, which was sterilized by UV irradiation and mixed with cooled Medium I in proportion of 1:1. The solution was continuously injected with N_2 for 60 min before sterilization to ensure the elimination of oxygen. The SRB were inoculated in a known proportion (1:50) into the mixed solution consisting of the experimental solution (3.5 wt% NaCl solution) and culture medium. Subsequently, the mixed solutions were incubated in a biochemical incubator at 30ºC. A certain quantity of the bacterial suspension was used to activate biotic medium. The change in the optical density (OD) with time was determined using a UV-2550UV spectrophotometer.

2.3 Growth cycle of SRB

The X70 steel specimens were immersed in the SRB-containing 3.5% NaCl medium and polarized by the applied potential of -0.55, -0.775, -0.85, -1.0 V_{SCE} and OCP. The SRB growth curve in 3.5% NaCl solution under various potentials was measured in 14 days by the optical density (OD) method with UV-2550 spectrophotometer.

2.4 Surface characterization

The X70 steel specimens were immersed into the SRB-containing media under various applied potentials. The samples were taken out on the 4^{th}, 7^{th}, 10^{th} and 14^{th} days. In order to ensure the integrity of the biofilm, the specimens were immobilized with glutaraldehyde (5 vol.%) for 4 h and dehydrated in ethanol (30, 50, 80, and 100 vol.%) for 15 min[33]. Biofilms and corrosion characteristics on the surface specimens were examined via SEM (SU-8010), EDS (Q500MW) and XRD (D8 Advance).

2.5 Electrochemical experiments

The EG&G PAR 2273 electrochemical station was used to perform the electrochemical experiments. Saturated calomel electrode (SCE), X70 steel and the platinum sheet were respectively served as the reference electrode, working electrode, and auxiliary electrode. The electrodes were exposed to ultraviolet light for at least 20 min before the experiment to ensure that they were not contaminated with other bacteria. The X70 steel was subjected to a constant potential polarization generated by PS-1 potentiostation. The applied polarization potentials were -0.55, -0.775, -0.85, -1.0 V_{SCE} and OCP, respectively. The X70 steel specimens measured for electrochemical impedance spectroscopy (EIS) were conducted on the 4^{th} , 7^{th}, 10^{th} and 14^{th} days, the frequency was 10^5 ~ 10^{-2} Hz and the sinusoidal excitation signal was 10 mV. The experimental results were analyzed by ZSimpWin software.

3. RESULTS

3.1 Measurements of E_{corr} and SRB growth curves

The corrosion potential (E_{corr}) of X70 steel in SRB-containing 3.5% NaCl solution is shown in Figure 1. The E_{corr} dropped sharply in the first day, decreased slightly from Day 2 to 4, then increased continuously from Day 5 to 9, and finally became stable approximately at -0.68 V_{SCE} from Day 10 to 14.

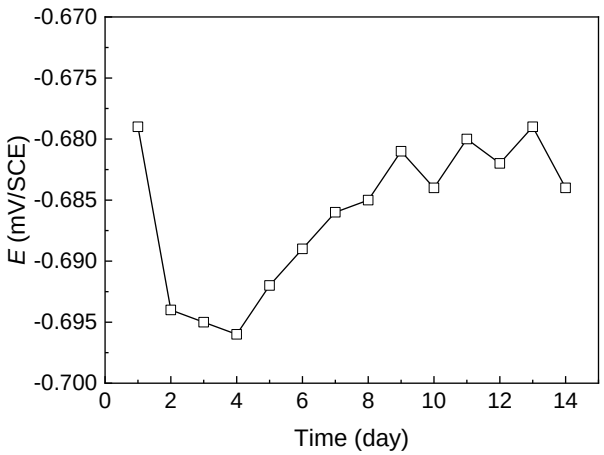

Figure 1. E_{corr} of X70 steel in 3.5% NaCl solution containing SRB.

The growth curves of SRB in 3.5% NaCl solution under various polarization potentials applied on X70 steel was shown in Figure 2. At OCP, the OD value rose faster in the first 6 days, indicating that SRB were in a logarithmic growth phase. Bacteria are highly active in the exponential stage, and there is a high rate of nutrient consumption and metabolite accumulation[34]. From Day 6 to 9, the OD value reached its maximum value, suggesting that SRB were in the stable growth phase. The OD value

decreased sharply from Day 10 to 14, indicating that SRB entered the decline period as a result of the nutrient depletion in the medium.

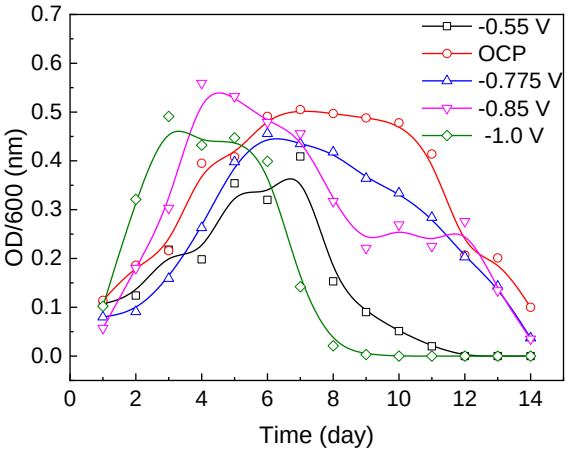

Figure 2. Growth curves of SRB under various applied potentials.

According to the E_{corr} result in the solution containing SRB, X70 steel was anodically polarized under -0.55 V_{SCE}, whereas X70 steel was cathodically polarized when the applied potentials were respectively -0.775, -0.85 and -1.0 V_{SCE}. All the growth curves of SRB rose firstly and then declined. When the applied potential was -0.55 V_{SCE}, the logarithmic growth phase was from the first day to 5th day. The OD value of active SRB reached the maximum value in the period from the 5th to 7th day. However, the increase in the OD value was the smaller than that under other applied potential. The OD value declined sharply from the 8th day and was almost close to zero on Day 10, indicating that anodic polarization was not conducive to SRB growth.

Under -0.775 V_{SCE}, the OD value increased slowly from 1 to 6 days and began to decline on the 7th day. Under -0.85 V_{SCE}, OD value increased obviously from the 1st to 4th day and reached its maximum, indicating that the potential of -0.85 V_{SCE} was conducive to SRB growth. Subsequently, OD value decreased and SRB entered the decline phase. When the applied potential was -1.0 V_{SCE}, the OD value peaked in the 3rd day and then the SRB entered the stable growth phase. The OD value gradually dropped to 0 from Day 8.

3.2 Surface characterization results

Figure 3 shows the XRD results of X70 steel immersed in the bacterial solution for 14 days under various applied potentials. FeS was detected in the corrosion product under all potentials. The corrosion products Fe_2O_3 and FeO were detected at OCP and -550mV, and Fe_3O_4 was also found at -550mV.

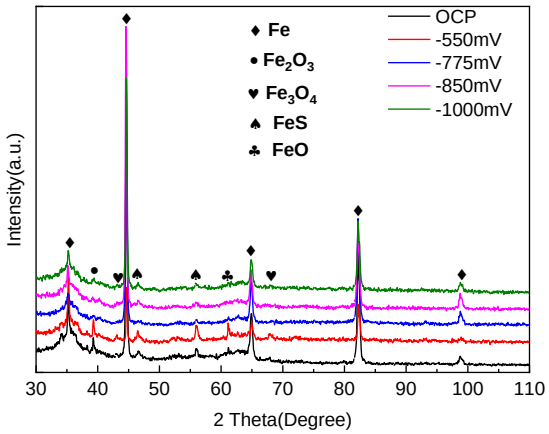

Figure 3. XRD patterns of X70 steel immersed in the bacterial solution for 7 days.

The SEM results of X70 steel immersed in the bacterial solution for 7 days under various applied potentials are shown in Figure 4. Many cracks were observed on the corrosion production film under -0.55, OCP and -0.775 V_{SCE}. These cracks might have formed during dehydration. The corrosion product film was the thickest under the OCP and the thinnest under -0.55 V (SCE). Under -0.85 and -1.0 V_{SCE}, the corrosion products were relatively integral without cracks. Figure 5 shows the SEM results of X70 steel after removing corrosion products. A number of obvious pitting were found under OCP, -0.55 and -0.775 V $_{SCE}$. A small number of shallow pitting were observed under -0.85 V_{SCE} and the slight uniform attack happened when the applied potential was -1.0 V $_{SCE}$.

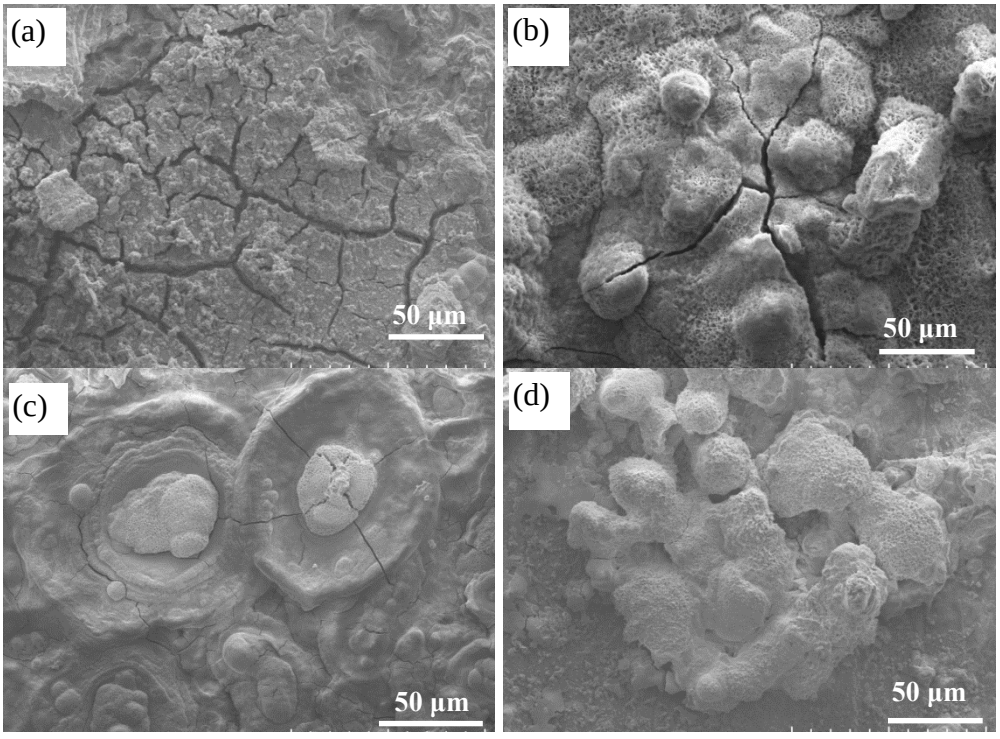

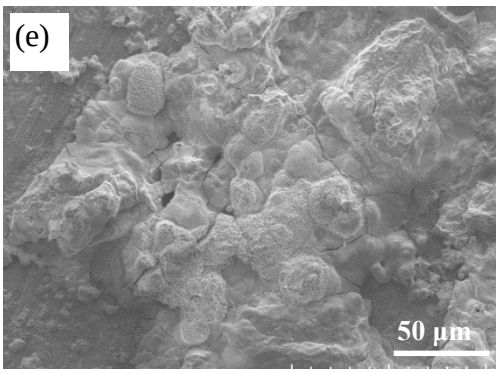

Figure 4. SEM images of X70 steel in the 3.5%NaCl containing SRB under various potentials for 7 days: (a) -0.55 V (SCE); (b) OCP; (c)-0.775 V (SCE); (d)-0.85 V (SCE); (e)-1.0 V (SCE).

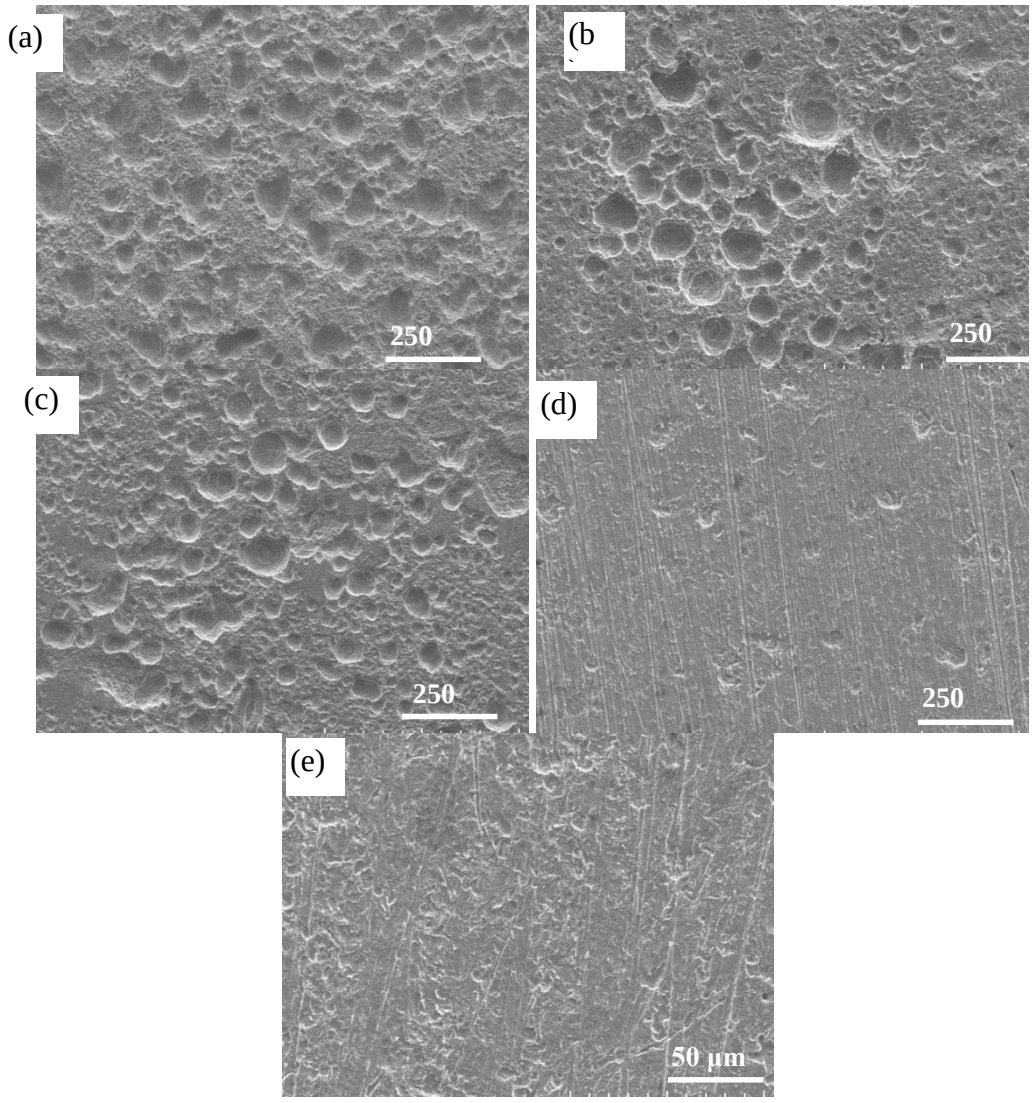

Figure 5. SEM images of X70 steel in the 3.5% NaCl containing SRB for 7 days after removing corrosion products: (a) -0.55 V (SCE); (b) OCP; (c)-0.775 V (SCE); (d)-0.85 V (SCE); (e)-1.0 V (SCE).

The SEM and EDS results of X70 pipeline steel immersed in the bacterial medium for 14 days under various applied potentials are shown in Figure 6. The corrosion products partly covered on the steel surface in clusters when the applied potential was -0.55 V_{SCE}. The corrosion product film was the thickest and the cracks were deeper under the OCP. Under the potential of -0.775 V_{SCE}, the corrosion products were the thinnest and many cracks were observed. In some places, the outer layer of the product had fallen off. Big bubbles were found on the steel surface under -0.85 and -1.0 V_{SCE}. When the potential was -1.0 V_{SCE}, the bubble had burst and the exposed internal substance had been corroded. The results of EDS showed that Fe and O were the major elements in the corrosion products. Therefore, iron oxides were the main corrosion products. Elements C and P came from the medium. In addition, the element S was detected when the applied potentials were respectively OCP, -0.55 and -0.775 V_{SCE} and its content was much higher than that of X70 steel, suggesting that S came from SRB metabolism. Element S was not found when the applied potentials were respectively -0.85 and -1.0 V_{SCE}.

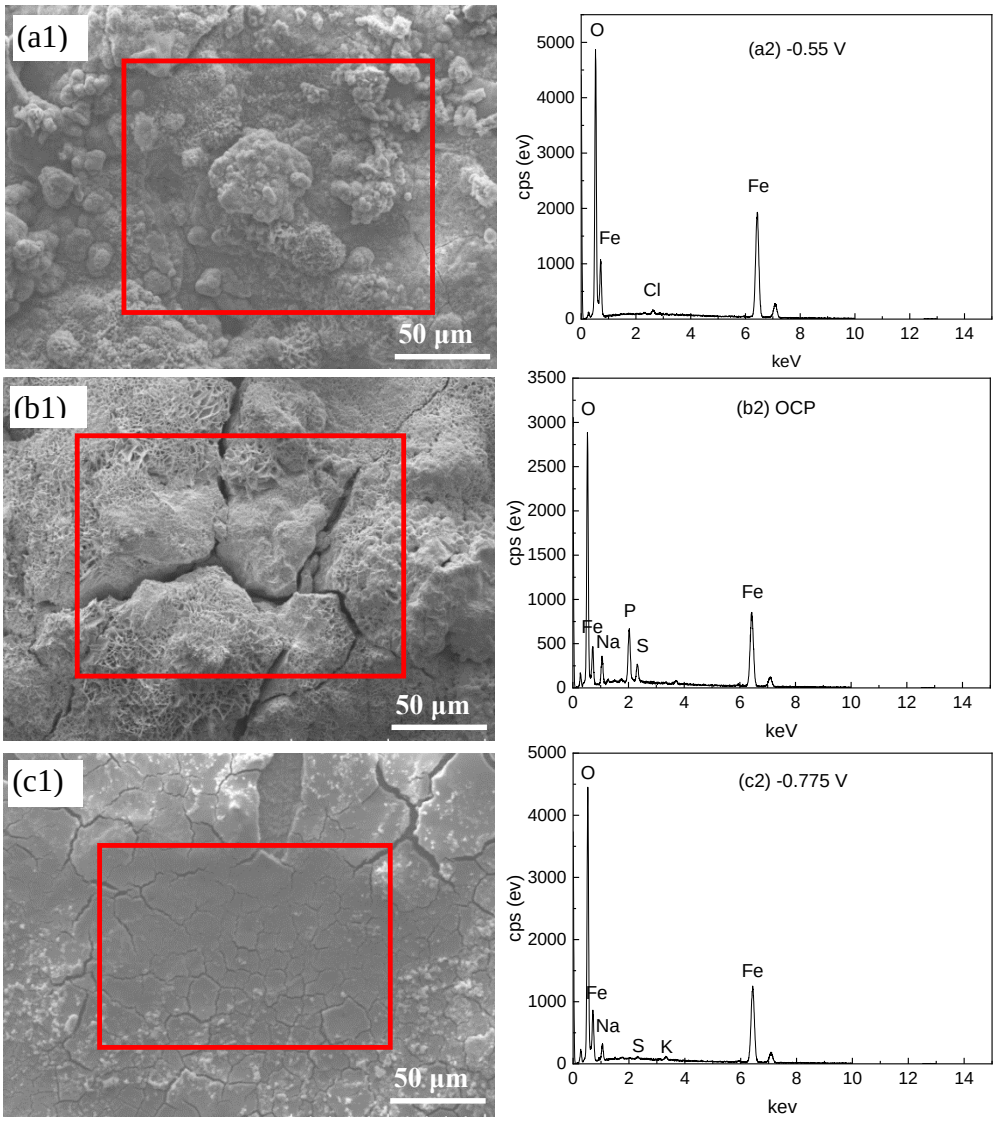

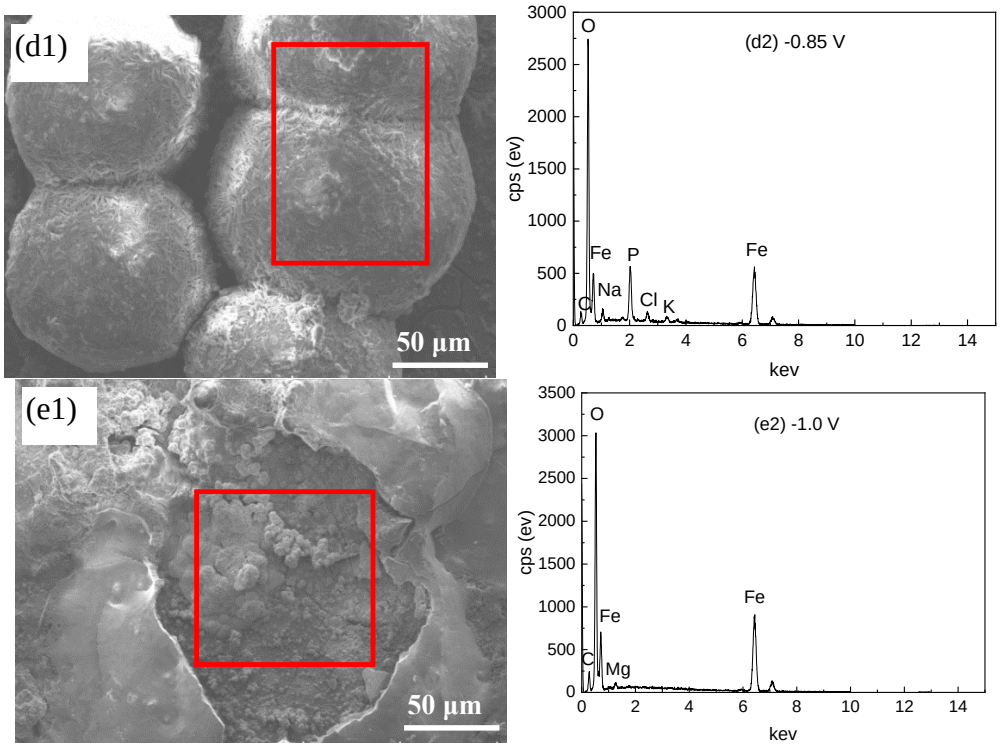

Figure 6. SEM images and EDS results of X70 steel in 3.5% NaCl containing SRB under various potentials for 14 days: (a1, a2) -0.55 V (SCE); (b1, b2) OCP; (c1, c2) -0.775 V (SCE); (d1, d2) -0.85 V (SCE); (e1, e2) -1.0 V (SCE).

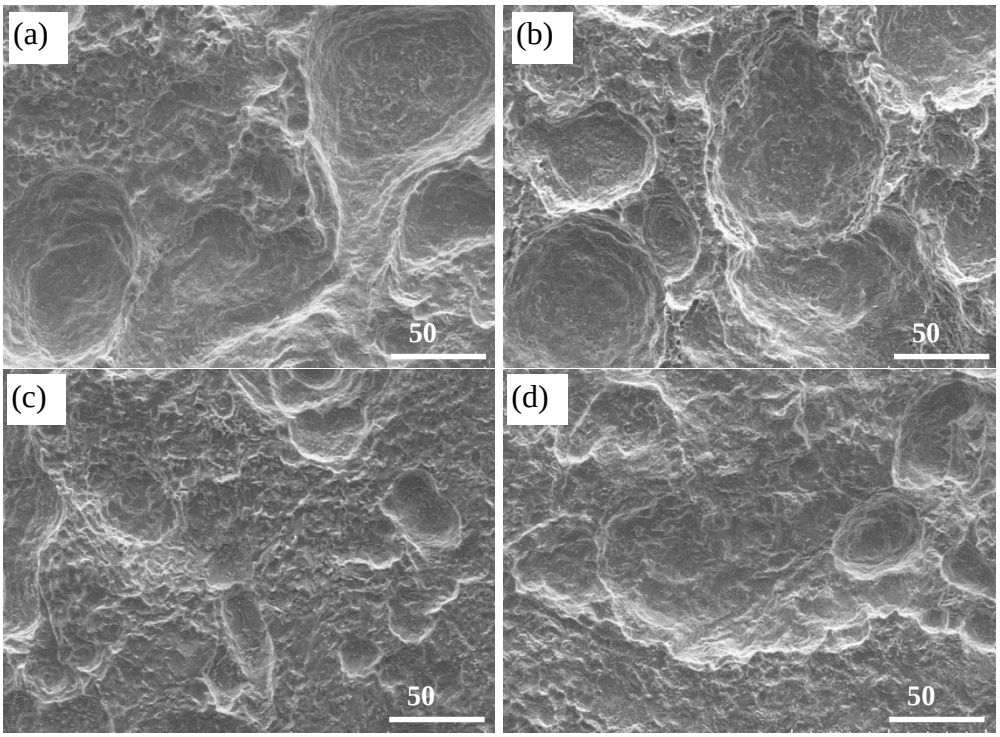

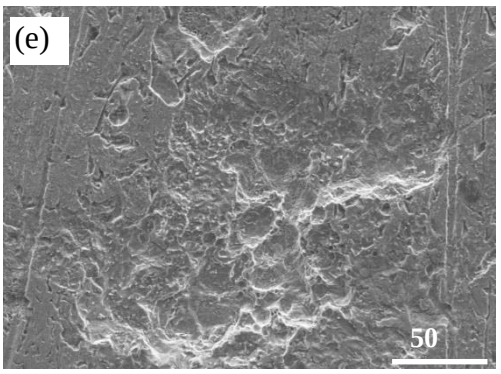

Figure 7. SEM images of X70 steel removing the corrosion products after immersing for 14 days: (a) -0.55 V (SCE); (b) OCP; (c)-0.775 V (SCE); (d)-0.85 V (SCE); (e)-1.0 V (SCE).

The SEM images the samples inmmersed in the bacterial solution for 14 days without corrosion products are shown in Figure 7. All the specimens were corroded and the pitting morphology were observed. Under OCP and -0.55 V_{SCE}, the specimens were seriously corroded and the pittings were wide in diameter and deep in depth. The specimen was slightly corroded when the potential was -1.0 V_{SCE}.

3.3 EIS of X70 steel in SRB medium under various potentials

Figure 8 shows the EIS plots of X70 steel in the bacterial 3.5% NaCl solution under various applied potentials. The Nyquist diagrams show a single capacitive loop in Day 4 and Day 7 under all applied potentials. While the polarization potential was -1.0 V_{SCE}, a inductance arc appeared at low frequency in Day 10 and Day 14, indicating that ions adsorption occurred on the electrode surface. In addition, in the 4^{th} and 7^{th} days, the largest radius of the capacitive arc appeared under -0.85 V_{SCE} and the corresponding phase angle was the closest to 90°. The smallest capacitive arc radius was observed under -1.0 V_{SCE}. It is generally believed that the magnitude of the capacitive arc is concerned with the corrosion of the metal. The larger the radius is, the better the corrosion resistance of the steel is. The phase angle reflects the completeness of the surface film. The closer to 90° the phase angle is, the more complete the surface film is. The capacitive arc radius in Day 4 was significantly greater than that in other days. In the 14^{th} day, the radius of the capacitive arc and phase angle values were the largest under the OCP and the radius was the smallest under -1.0 V_{SCE}. The peak of phase angle moved to the intermediate frequency region under the potential of -0.85 V_{SCE}.

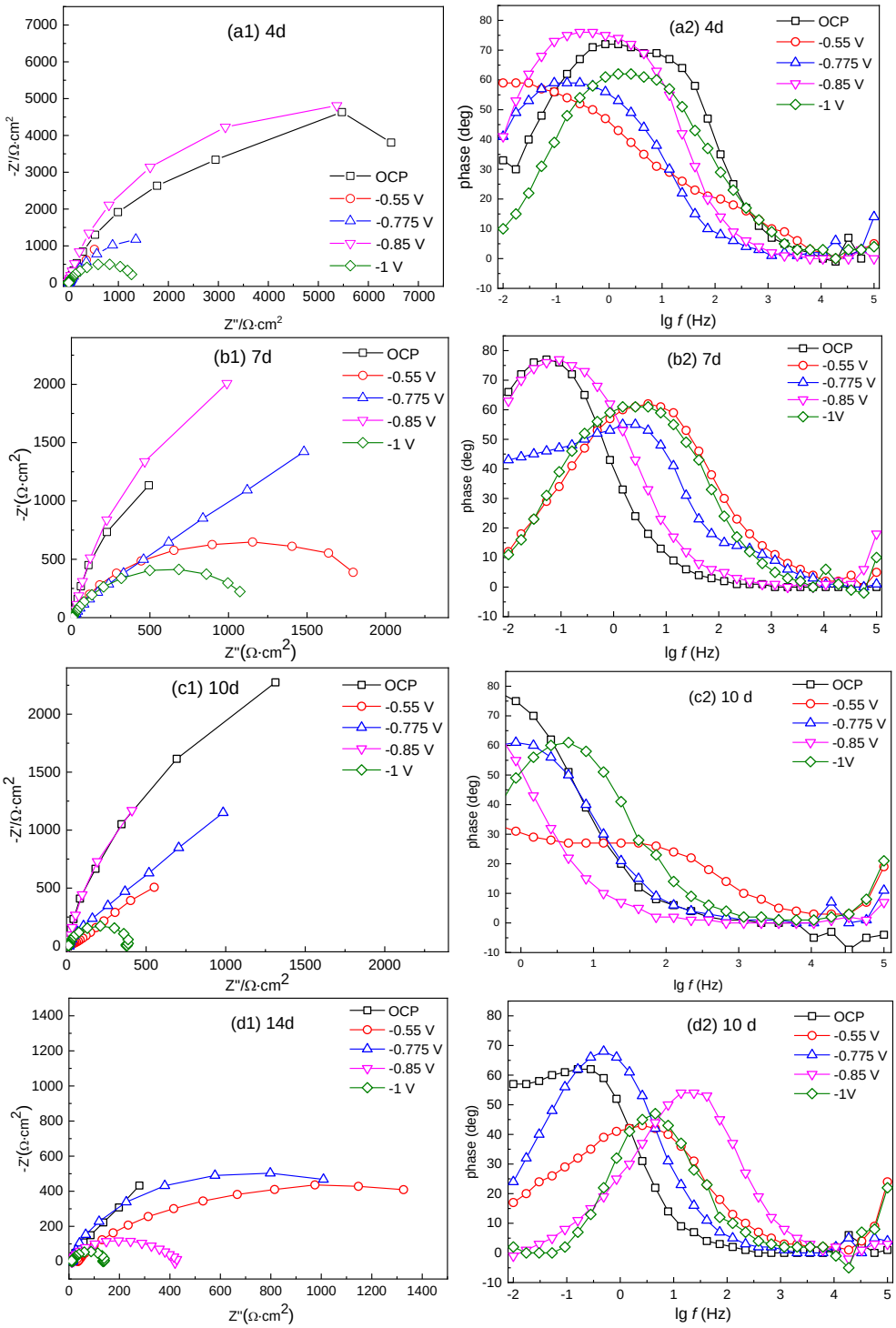

Figure 8. Nyquist and Bode plots of X70 steel in 3.5%NaCl solution containing SRB under various potentials: (a1, a2) 4 d; (b1, b2) 7 d; (c1, c2) 10 d; (d1,d2) 14 d.

4. DISCUSSION

4.1 Effects of applied potentials on the SRB growth

The results of E_{corr} and the growth curves of SRB indicated that SRB activity was closely related to E_{corr} under the OCP. As immersed in the SRB medium, the surface of X70 steel was

activated, resulting in the formation of countless activation sites on the steel surface and the rapid negative shifting of E_{corr} in the 1st da. When SRB was in logarithmic growth period, the bacteria colonizing on the electrode surface was inadequate to form a complete protective film, thus decreasing E_{corr}. When SRB was in stable growth period, the quantity of SRB peaked and the corrosion product scale formed on the electrode surface was thicker. The corrosion product scale acted as a barrier layer preventing the solution from diffusing onto the electrode surface, so E_{corr} increased continuously. When the SRB entered the decline phase, the electrochemical reactions on the electrode surface achieved the dynamic equilibrium, and E_{corr} was basically stable at -0.68 V_{SCE}.

The growth curves of SRB under various applied potential showed that the anodic polarization potential was not conducive to SRB growth when the applied potential was -0.55 V_{SCE}. When microbial cells were exposed to an electric field, the arrangement of molecules in the cell membrane was affected by the electric field. The trans-membrane voltage was thus generated on both sides of the cell membrane and the permeability and conductivity of the cell membrane were significantly changed. When the trans-membrane voltage exceeded the voltage that the microorganism could withstand, the cells lose their activity and die[35,36]. Jia et al.[37] studied the effect of ferrous ion concentration on SRB activity and found that both sessile and planktonic cell increased with the Fe^{2+} concentration. This is inconsistent with the results of our work. This may be because Fe^{2+} was obtained by adding ferrous ammonium sulfate stock solution in his experiment, so sulfate ions were introduced, which promoted the growth of SRB.

When the cathodic potential was applied, the logarithmic growth phase of SRB was shortened and the bacteria entered the decline phase prematurely with the cathodic polarization potential moving negatively. The results indicated that cathodic current not only promoted SRB reproduction, but also hastened the death of SRB. Most of SRB cells in the logarithmic growth phase were in a state of mitosis [35] and the cell membrane was sensitive to the applied electric field. The mitotic cycle of cells was shortened by the stimulation of the applied cathodic electric field and the rate of cell division increased, thereby promoting the reproduction rate of microorganisms[38]. The result was consistent with the results of Guan [22]. When the cathodic current exceeded the tolerance of the bacteria, the cells become inactivated, just like the case of anodic polarization.

Some scholars believed that pH increase and the alkaline environment caused by the negative potential shift were not conductive to SRB growth[22,39]. De Romero [40,41] studied the influences of polarization potential on the growth of SRB in the potential range from -1.5 to -2.1 V_{CSE} and found that the bacterial concentration decreased by two orders of magnitude and that the pH value increased from 7 to 9. They argued that the metal/solution interface was alkaline which killed SRB. In fact, the pH in the metal/solution interface was difficult to be increased above 10[9,22,32]. Our previous work has shown that SRB could survive well in the medium with a pH range of 6-10[42]. In addition, the alkalization theory could not interpret the inactivation of SRB under the anode polarization potential. Therefore, the effect of CP on SRB growth was achieved by the electric field on bacterial mitosis, other than the increase in the pH of the solution.

4.2 Effect CP on the electrochemical behavior

EIS is a useful method to explore the electrochemical reaction mechanism. The electrochemical corrosion system is usually composed of several independent reaction processes. The parameters of each reaction process can be obtained by analyzing response signals. Figure 9 shows the equivalent circuits fitting for the EIS of X70 steel in bacterial 3.5% NaCl solution. The double-layer circuit model is more suitable for fitting the EIS results at any potential in bacterial 3.5%NaCl solution, because of the coverage of biofilm and FeS on the electrode surface. The parameters in Fig. 8 are provided as follows. R_s is the solution resistance; Q_{dl} and R_{ct} are the constant phase angle element of the electric double layer and is the charge transfer resistance, respectively; Q_f and is R_f are respectively the constant phase angle element and resistance related to the biofilm/corrosion product film; W is the Warburg impedance; L is the inductance. The capacitive elements commonly refer to the constant phase angle that can reflect the dispersion effects [43,44]. The dispersion degree is represented by the index n. Warburg impedance represents that the electrochemical process is controlled by diffusion and inductance usually represents the adsorption. The fitting results of EIS are shown in Table 1.

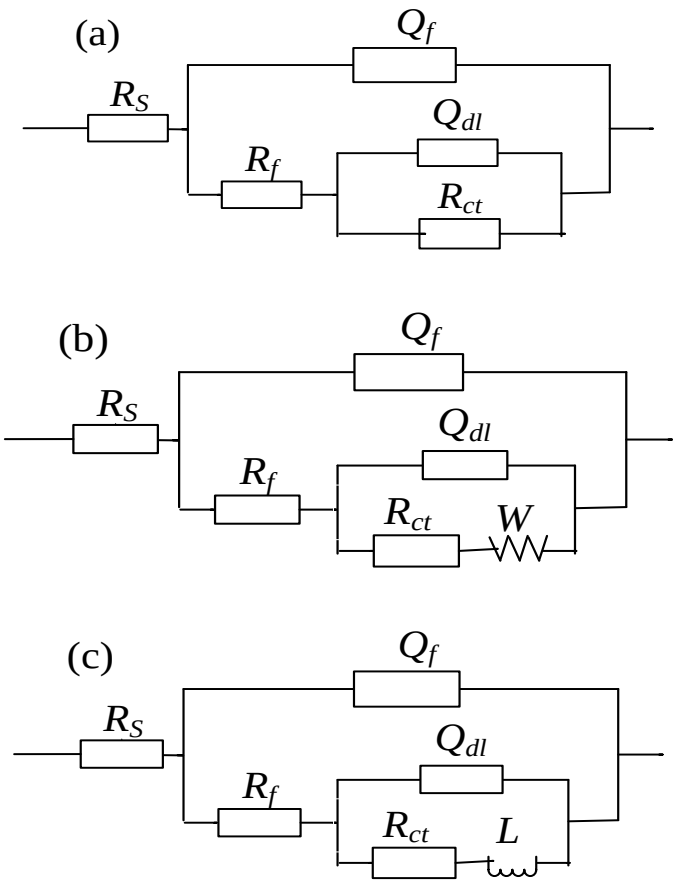

Figure 9. Equivalent circuits of EIS: (a) OCP and -0.85 V; -0.55 V in Day 7 and Day 10; -0.775 V in Day 4 and Day 14; -1.0 V in Day 4 and Day 7; (b) -0.55 in Day 4; -0.775 V in Day 7 and Day 10; (c) -1.0 V in Day 10 and Day 14.

Table 1. Fitting results of electrochemical impedance spectroscopy

Time d	E V	R_s $\Omega\cdot cm^2$	Q_f Ω^{-1} cm^{-2} s^n	n_f	R_f $\Omega\cdot cm^2$	Q_{dl} Ω^{-1} cm^{-2} s^n	n_{dl}	R_t, $\Omega\cdot cm^{-2}$	$W(\Omega\cdot cm^2)$/ $L(H\cdot cm^2)$
4	-0.55	7.25	1.13×10^{-4}	---	4.32	1.45×10^{-2}	0.83	6003	W=0.010
	OCP	9.03	5.31×10^{-4}	0.89	622.7	1.8×10^{-4}	0.76	9799	
	-0.775	14.46	2.96×10^{-3}	0.74	1089	6.34×10^{-4}	1	2898	
	-0.85	10.02	7.97×10^{-4}	0.96	319	3.69×10^{-4}	0.79	11290	
	-1.0	5.65	1.73×10^{-4}	1	4.28	1.23×10^{-3}	0.72	1446	
7	-0.55	8.4	1.22×10^{-3}	0.72	1927	1.79×10^{-3}	0.93	239.8	
	OCP	7.62	1.07×10^{-2}	0.71	76.99	1.42×10^{-2}	0.97	2879	
	-0.775	13.17	5.78×10^{-5}	0.99	7.39	8.98×10^{-4}	0.84	306.8	$W=1.7\times10^{-3}$
	-0.85	12.3	3.87×10^{-3}	0.87	35.78	1.19×10^{-3}	----	7521	
	-1.0	5.85	3.65×10^{-4}	1	9.47	1.46×10^{-3}	0.68	1277	
10	-0.55	12.13	1.29×10^{-3}	0.68	31.83	6.12×10^{-3}	0.54	10120	
	OCP	6.86	4.41×10^{-3}	---	0.750	4.03×10^{-3}	0.92	6599	
	-0.775	12.82	1.99×10^{-3}	0.82	9.76	3.20×10^{-4}	----	368.5	$W=2.1\times10^{-3}$
	-0.85	10.79	3.5×10^{-2}	0.7	345	1.34×10^{-2}	---	4206	
	-1.0	13.24	3.62×10^{-4}	0.42	11.94	5.67	---	401.9	$L=5.18\times10^{-5}$
14	-0.55	36.2	6.52×10^{-4}	0.73	323.3	1.29×10^{-3}	0.42	1925	
	OCP	9.95	1.06×10^{-2}	0.85	6891	8.79×10^{-3}	0.84	197.7	
	-0.775	11.69	2.81×10^{-3}	0.79	7.42	8.17×10^{-4}	1	1332	
	-0.85	11.05	3.65×10^{-4}	0.86	187.5	2.08×10^{-3}	0.79	222.1	
	-1.0	16.44	9.01×10^{-4}	0.35	13.23	8.37×10^{-4}	---	134.5	$L=9.16\times10^{-5}$

Under the OCP, the steel surface was simultaneously subjected to two reactions: the cathode and the anode reactions. EIS were the combined result of the two reactions. The R_{ct} of an electrochemical reaction can be expressed as:

$$\frac{1}{R_{ct}} = \frac{1}{R_{ct,a}} + \frac{1}{R_{ct,c}}, \quad (1)$$

where $R_{ct,c}$ and $R_{ct,a}$ are respectively the charge transfer resistance of cathode and anode reactions.

When the electrode is cathodically polarized, with the applied potential moving negatively, $R_{ct,a}$ increases, but $R_{ct,c}$ gradually decreases. When CP increased to a certain level, $R_{ct,a}$ is large enough that can be ignored, thus $R_{ct,c}$ is equal to R_{ct}. The fitting results of $R_{ct,}$ under various CP are summarized in Figure 10. Under the OCP, the value of R_{ct} reached its maximum at this potential on the 4th day. This can be attributable to greater activity of SRB in the logarithmic growth phase. At this period, the bacterial cells with negatively charged and their metabolites were attached on the metal surface. Meanwhile, electric charge was transferred to the electrode, changing the metal/solution interface and promoting the charge transfer. R_{ct} decreased obviously from the 4th day to the 7th day and then remained stable in the remaining experimental period. As the applied potential was -0.775 V(SCE), R_{ct} was much lower than that under the OCP, indicating that anode reaction could not be suppressed under this potential and that X70 steel was in an insufficient CP condition. The R_{ct} for the potential of -0.85 V_{SCE} showed a linear decline. In the first 4 days, R_{ct} value was greater than that under the OCP, suggesting that the anodic reaction was suppressed and that X70 steel was in a good CP condition. According to the growth curves of SRB, the corrosion was promoted by bacteria metabolism. Then, R_{ct} value continuously decreased and was only slightly higher than that under the OCP in the 10th day, indicating that bacterial corrosion was exacerbated. In the 14th day, R_{ct} was much lower than that under

the OCP. Based on the SEM results (Fig. 5 (d1)), SRB metabolites (such as H_2S) in the solution promoted the hydrogen evolution reaction. Little and Lee[45] indicated that general corrosion rates in the presence of SRB were not proportional to the number of bacterial cells. When the applied potential reached -1.0 V_{SCE}, R_{ct} remained to be low due to hydrogen evolution reaction and X70 steel was in an overprotected condition [46]. Liu [32] proved that under the potential of -0.92 V_{SCE}, thin biofilms were attached to the steel surface but the biofilms were not evenly distributed. The number of SRB and the deposits density on the electrode surface decreased under -1.0 V_{SCE}. The bare metal surface also facilitated hydrogen absorption, leading to local acidification, which in turn promoted pitting. Esquivel[47] studied the corrosion behavior of X52 steel in SRB-containing medium for 30 days and found that the CP potential of -0.95 V_{CSE} was still inadequate.

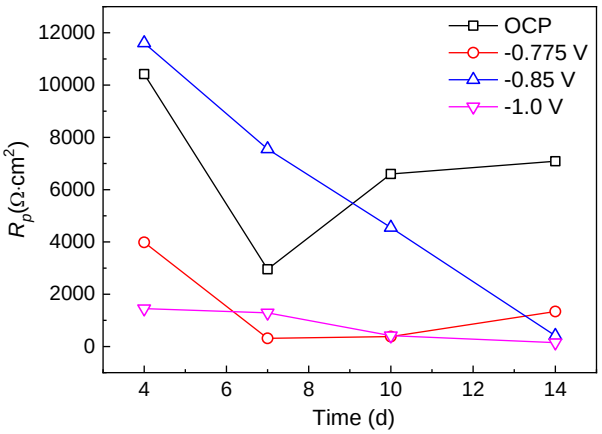

Figure 10. Polarization resistance in the experimental period.

4.3 Corrosion mechanism of X70 steel under the synergistic action of SRB and CP

Various types of iron sulfide might form on the steel surface when it was immersed in the bacterial medium without CP. The corrosion product $Fe_{1+x}S$ could provide protection for the steel at the beginning. But when the corrosion product layer became thicker and cracks occurred, the corrosion rate increased. SEM results showed that in Day 7, the corrosion product layer was very thick and cracks appeared. The reactions on the surface of X70 steel in a bacterial 3.5% NaCl solution are provided as[48]:

$$4Fe \rightarrow 4Fe^{2+} + 8e^- \quad (2)$$

$$8H_2O \rightarrow 8OH^- + 8H^+ \quad (3)$$

$$8H^+ + 8e^- \rightarrow 8[H] \quad (4)$$

$$SO_4^{2-} + 8[H] \rightarrow \text{MIC} \rightarrow S^{2-} + 4H_2O \quad (5)$$

$$Fe^{2+} + S^{2-} \rightarrow FeS \quad (6)$$

$$3Fe^{2+} + 6OH^- \rightarrow 3Fe(OH)_2 \quad (7)$$

Overall reaction: $$4Fe + SO_4^{2-} + 4H_2O \rightarrow FeS + 3Fe(OH)_2 + 2OH^- \quad (8)$$

Dinh et al. [26] suggested that Fe^0 could be utilized directly by SRB as an electron donor and therefor sulfate reduction was much quicker than traditional hydrogen-cleaning process.

When X70 steel was cathodically polarized, the anodic reaction was suppressed and Fe^0 could not be used as the electron donor. At this point, the SRB was able to obtain electrons from the excess cathodic current and be metabolized. With the moving negatively of CP potential, the number of excess electrons increased and SRB metabolism was accelerated, so the peak of SRB propagation obtained prematurely. When the potential was -0.85 V_{SCE}, the quantity of SRB was the highest, but EIS results showed that the charge transfer resistance (R_{ct}) was the largest during the SRB growth period. This indicates that CP can mitigate SRB corrosion. The SRB cell surface was negatively charged through the ionization of phosphate and carboxyl substituents on the outer surface[49]. When CP was applied, the steel surface was negatively charged and bacterial cells were repelled during their attachment process. The SEM results also showed that the corrosion products scale was thinner when CP was applied. Lv [50] proved that the surface of SRB cells had a negative charge of 3mV. Therefore, the adhesion of SRB to X70 steel surface was affected by electrostatic repulsion under the cathodic polarization. Hong [51] found that about 80% of the bacteria were promoted to be separated from the metal surface, whereas 20% of the bacteria were still on the metal surface under the cathode current of 15 μA/cm^2 when electrostatic repulsion and electrophoretic repulsion were applied. In contrast, the remaining bacteria on the steel surface were gradually inactive in the presence of anode current. As SRB entered the decline phase, charge transfer resistance decreased continuously. This is attributed to H_2S generated by SRB metabolism leading to hydrogen evolution: [52]:

$$2H_2S + 2e^- \rightarrow 2HS^- + H_2 \quad (9)$$

$$2HS^- \rightarrow 2H^+ + 2S^{2-} \quad (10)$$

When the applied potential reached -1.0 V_{SCE}, X70 steel was in an overprotected condition. The hydrogen bubbling ruptured and X70 steel was exposed to the corrosive medium. SEM results (Figure 6 e) showed that slight pitting occurred on the surface of X70 steel. This corrosion was in agreement with the previous reports by Liu [32]. In this study, the SRB entered the decline phase prematurely under -1.0 V_{SCE}, and the quantity of bacterial on the electrode surface decreased, thus mitigating the microbial corrosion of X70 steel. In addition, Mg^{2+} was detected in the corrosion products under -1.0 V_{SCE}, indicating that the increasing in solution alkalinity led to the deposition of magnesium:

$$Mg^{2+} + 2OH^- \rightarrow Mg(OH)_2 \quad (11)$$

Bacterial cells can use divalent cations (Ca^{2+} and Mg^{2+}, for example) as intermediaries. The deposition of Ca^{2+} and Mg^{2+} lead to a decline in localized concentration, so bacteria cannot obtain them and the corrosion rate was reduced [28]. The application of cathodic protection led to the transformation of sulfide rusts into carbonates rusts[53].

5. CONCLUSIONS

Polarization potential has significant influence on SRB growth cycle. Under the anodic polarization potential, SRB reproduction is suppressed and rapidly enters the decline phase after the logarithmic growth phase. At a lower CP potential (-0.85 V), the mitotic cycle of SRB is accelerated and reproduction is promoted. At a higher CP potential (-1.0 V), SRB rapidly enters the death phase.

The growth cycle of SRB also has significant influence on the CP efficiency. During SRB growth phase, the excess electrons of CP are directly utilized by SRB as electron donors to metabolize. CP current repels the electronegative SRB, which reduces the adhesion of SRB to steel surface. CP and SRB synergistically mitigate the steel corrosion. When SRB enters the death stage, H_2S, the metabolite of SRB, acts synergistically with CP to promote hydrogen evolution, and CP promotes SRB corrosion.

ACKNOWLEDGEMENTS
We are grateful to Chunhui Program of the Ministry of Education of China and the Key Project of Education Department of Liaoning Province of China (Grant number: L2017LZD004) for their financial support.

References

1. A. Q. Fu, Y. F. Cheng, *Can. Metall. Quart.*, 51 (2012**)** 81.
2. A. Eslami, R. Kania, B. Worthingham, G. V. Boven, R. Eadie, W. Chen, *Corrosion*, 69 (2013) 1103.
3. X. Chen, C. W. Du, X. G. Li, Y. Z. Huang, *J. appl. Electrochem.*, 39 (2009) 697.
4. M. C. Yan, J. Q. Wang, E. H. Han, W. Ke, *Corros. Sci*., 50 (2008) 1331.
5. X. Chen, X. G. Li, C. W. Du, Y. F. Cheng, *Corros. Sci.*, 51 (2009) 2242.
6. H. C. Qian, L. T. Wang, H. R. Wang, W. R. Zheng, C. W. Du, *J. Mater. Eng. Perform*., 25 (2016) 4657.
7. A. Fatehi, A. Eslami, M. A. Golozar, K. Raeissi, R. Ashari, *Corros.*, 75 (2019).4
8. M. C. Yan, J. Xu, L. B. Yu, T. Q. Wu, C. Sun, W. Ke, *Corros. Sci.*, 110 (2013) 23.
9. X. Chen, G. F. Wang, F. J. Gao, Y. L. Wang, C. He, *Corros. Sci*., 101 (2015) 1.
10. Z. Y. Liu, X. G. Li, C. W. Du, G. L. Zhai, Y. F. Cheng, *Corros. Sci*., 50 (2008) 2251.
11. A. Q. Fu, Y. F. Cheng, *Corros. Sci*., 52 (2010) 2511.
12. A. Eslami, R. Kania, B. Worthingham, G. V. Boven, G. Eadie, W. Chen, *Corros. Sci.*, 53 (2011) 2318.
13. J. G. Kim, Y. W. Kim, *Corros. Sci.*, 43 (2001) 2011.
14. R. G. Esquivel, G. Z. Olivares, H. Gayosso, A. G. Trejo, *Mater. Corros.*, 62 (2011) 61.
15. H. Liu, Y. F. Cheng. *Colloids Surf. B*, 190 (2020) 110899.
16. H. Liu, T. Y. Gu, G. Zhang, H. F. Liu, Y. F. Cheng, *Corros. Sci.*, 136 (2018) 47.
17. Q. Li, J. H. Wang, X. T. Xing, W. B. Hu, *Bioelectrochemistry*., 122 (2018) 40.
18. E. Ubong, F. Omar, S. Jerzy, *Eng. Fail. Anal.*, 93 (2018) 111.
19. H. Liu, L. Huang, Z. Huang, J. Zheng, *Mater. Corros*., 58 (2007) 44.
20. B. Anandkumar, R. P. George, S. Maruthamuthu, N. Parvathavarthini, U. K. Mudali, *Corros. Re.*, 34 (2016) 1.
21. A. Fatehia, A. Eslamia, M. A. Golozara, K. Raesia, R. Asharia, *J. Mater. Eng. Perform.*, 122 (2018) 40.
22. F. Guan, X. F. Zhai, J. Z. Duan, M. X. Zhang, B. R. Hou, *Plos. One.*, 11 (2016) 1.
23. S. Yuan, B.iang, Y. Zhao, S. O. Pehkonen, *Corros. Sci.*, 74 (2013) 353.
24. D. Xu, Y. Li, T. Gu, *Bioelectrochemistry*., 110 (2016) 52.
25. Q. Bao, D. Zhang, D. Lv, P. Wang, *Corros. Sci.*, 65 (2012) 405.
26. P. Bai, H. Zhao, S. Zheng, C. Chen, *Corros. Sci*., 93 (2015) 109.
27. H. T. Dinh, J. Kuever, M. Mussmann, A. W. Hassel, M. Stratmann, F. Widdel, *Nature.*, 427 (2004) 829.

28. R. G. J. Edyvean, A. D. Maines, C. J. Hutchinson, N. J. Silk, L. V. Evans, *Int. Biodeterior. Biodegradation.*, 29 (1992) 251.
29. B. Little, P. Wagner, K. Hart, R. Ray, *Corrosion*, 96 (1996) 278.
30. G. Nekoksa, B. Gutherman, Cathodic protection criteria for controlling microbially influenced corrosion in power plants., Electric Power Research Institute, Palo Alto, CA, USA, 1991, 7312.
31. M. E. Shirtliff, R. A. Bargmeye, A. K. Camper, *Appl. Environ. Microbiol*., 71 (2005) 6379.
32. T. Liu, Y. F. Cheng, *J. Alloy. Compd*., 729 (2017) 180.
33. P. J. Antony, S. Chongdar, P. Kumar, *Metall. Mater. Trans. A*., 52 (2007) 3985.
34. J. Chen, J. J. Wu, P. Wang, D. Zhang, S. Q. Chen, F. Q. Tan, *J. Mater. Eng. Perform.*, (2019)1469.
35. M. M. Góngora-Nieto, F. Younce, G. M. Hyde, *Innov. Food. Sci. Emerg*., 3 (2002) 337.
36. P. She, B. Song, X. H. Xing, M. V. Loosdrecht, *Biochem. Eng. J.*, 28 (2006) 23.
37. R. Jia, D. Wang, P. Jin, T. Unsal, D. Q. Yang, J. K. Yang, D. K. Xu, *Corros. Sci.*, 153 (2019) 127.
38. F. L. Zhong, H. B Cao, X. G. Li, *Bulletin of microbiology*., 28 (2001) 77.
39. W. H. Hartl, G. Hernandez, H. A. Videla, *Corros. Rev*., 12 (1994) 29.
40. M. De Romero, O. De Rincón, M. anz, B. Rincón, L. Ocando, W. Campos, M. Bracho,. Evaluation Of Cathodic Protection In Presence Of Sulfate Reducing Bacteria Mixed Cultures., NACE International, New Orleans, USA, 2008**,** 8504.
41. M. De Romero, O. De Rincón, L. Ocando, Cathodic Protection Efficiency In The Presence of SRB: State of The Art., NACE International, Atlanta, USA, 2009, 9407.
42. X. Li, X. Chen, W. Q. Song, J. X. Yang, M. Wu. *J Chin Soc Corr Pro*., 38 (2018) 565.
43. B. Hirschorn, M. E. Orazem, B. Tribollet, V. Vivier, I. Frateur, M. Musiani. *Electrochim. Acta*., 55 (2009) 21.
44. Y. Huang, H. Shih, F. Mansfeld. *Mater. Corros.*, 61 (2010) 4.
45. B.J. Little, J.S. Lee, *Int. Mater. Rev.*, 59 (2014) 384.
46. M. Wu, D. X.Sun , K. Gong. *Eng. Fail. Anal.*, 109 (2020).
47. R. G. Esquivel, G. Z. Olivares, M. Gayosso, A. G. Trejo, *Mater. Corros.*, 62 (2011) 61.
48. X. Yang, J. Shao, Z. Liu, D. Zhang, X. Li, *Corros. Sci.*, 173 (2020) 108746.
49. W. W. Wilson, M. M. Wade, S. C. Holman, F. R. Champlin, *J. Microbiol. Meth*. 43 (2001) 1.
50. D. Lv, Y. Wang, D. Zhang, *Corros. Sci. Prot Technol.*, 26 (2014) 487.
51. S. H. Hong, J. Jeong, S. Shim, H. Kang, S. Kwon, K. H.Ahn, J. Yoon, *Biotechnol. Bioeng.*, 100 (2008) 379.
52. F. Kajiyama, K.Okamura, *Corrosion*, 55 (2011) 74.
53. P.Refait, M. Jeannin, R. Sabot, H. Antony, S. Pineau, *Corros. Sci.*, 71 (2013) 32.

© 2021 The Authors. Published by ESG (www.electrochemsci.org). This article is an open access article distributed under the terms and conditions of the Creative Commons Attribution license (http://creativecommons.org/licenses/by/4.0/).